nature materials

ARTICLES

PUBLISHED ONLINE: 25 JULY 2016 | DOI: 10.1038/NMAT4704

Decoupling a hole spin qubit from the nuclear spins

Jonathan H. Prechtel[1], Andreas V. Kuhlmann[1], Julien Houel[1,2], Arne Ludwig[3], Sascha R. Valentin[3], Andreas D. Wieck[3] and Richard J. Warburton[1]*

A huge effort is underway to develop semiconductor nanostructures as low-noise hosts for qubits. The main source of dephasing of an electron spin qubit in a GaAs-based system is the nuclear spin bath. A hole spin may circumvent the nuclear spin noise. In principle, the nuclear spins can be switched off for a pure heavy-hole spin. In practice, it is unknown to what extent this ideal limit can be achieved. A major hindrance is that p-type devices are often far too noisy. We investigate here a single hole spin in an InGaAs quantum dot embedded in a new generation of low-noise p-type device. We measure the hole Zeeman energy in a transverse magnetic field with 10 neV resolution by dark-state spectroscopy as we create a large transverse nuclear spin polarization. The hole hyperfine interaction is highly anisotropic: the transverse coupling is <1% of the longitudinal coupling. For unpolarized, randomly fluctuating nuclei, the ideal heavy-hole limit is achieved down to nanoelectronvolt energies; equivalently dephasing times up to a microsecond. The combination of large T_2^* and strong optical dipole makes the single hole spin in a GaAs-based device an attractive quantum platform.

A localized, single spin is a small and fast qubit. The exchange interaction between neighbouring spins facilitates two-qubit operations[1]. Implementation in a semiconductor benefits from advanced semiconductor heterostructures and nanofabrication; implementation in a GaAs-based heterostructure, the cleanest and most versatile semiconductor system, by trapping the spin to a quantum dot also facilitates the creation of a spin/photon interface. A stumbling block is that the nuclear spins in the quantum dot lead to a rapid loss of electron spin coherence (both T_2 and T_2^* processes)[2–4]. This has motivated interest in isotopically pure silicon, a nuclear spin-free host[5]. However, the large effective mass of a conduction electron in Si demands much smaller structures and lower operating temperatures; the valley degeneracy is an additional complication[6]; the strong optical dipole is lost. An approach that retains the GaAs system while suppressing the interaction of the spin qubit to the nuclear spins is attractive. It is worthwhile to re-address the interaction between an electron spin in a GaAs-based system, here an InGaAs quantum dot, and the host nuclear spins, the hyperfine interaction.

The electron states in a self-assembled quantum dot (Fig. 1a) are constructed from atomic *s* orbitals (Fig. 1b). The large amplitude of the *s* orbital at the location of each nucleus *i* results in a Fermi contact hyperfine interaction for an electron spin $\mathbf{S}$ with N nuclear spins $\mathbf{I}_i$

$$H_{\mathrm{hf}}^{e} = \Omega \sum_{j=1}^{N} A_{\mathrm{e}}^{j} |\Psi_{\mathrm{e}}(\mathbf{R}_j)|^2 (I_z^j S_z + I_x^j S_x + I_y^j S_y) \qquad (1)$$

A_{e}^{j} is the coupling coefficient, Ψ_{e} is the electron envelope function and Ω is the unit cell volume. The nuclei create an effective magnetic field, the Overhauser field B_N, which fluctuates in time resulting in spin dephasing[2,3]. For self-assembled quantum dots, $N \sim 10^5$ and $B_N \sim 20$ mT resulting in an energy fluctuation in the electron Zeeman energy of $\delta E_z \simeq 0.6\,\mu$eV and $T_2^* \sim 1$ ns. This dephasing can be suppressed only by 'narrowing' the nuclear spin distribution, ideally by preparing the nuclei in a z-eigenstate.

A hole is the absence of an electron in an otherwise occupied valence level. A hole spin has a fundamentally different hyperfine interaction to the electron spin. The valence states are constructed from atomic *p* orbitals with zero wavefunction amplitude at the location of the nuclei (Fig. 1b). The Fermi contact hyperfine interaction is therefore suppressed[4,7,8]. The dipole–dipole part of the hyperfine interaction remains[7–10]. For a pure heavy-hole (HH) state the hyperfine interaction has an Ising form,

$$H_{\mathrm{hf}}^{\mathrm{HH}} = \Omega \sum_{j=1}^{N} A_{\mathrm{h},z}^{j} |\Psi_{\mathrm{h}}(\mathbf{R}_j)|^2 I_z^j S_z \qquad (2)$$

$A_{\mathrm{h},z}^{j}$ is the coupling coefficient, Ψ_{h} is the hole envelope function, and $S_z = \pm 1/2$ represents $J_z = \pm 3/2$. The absence of transverse terms means that the heavy-hole spin experiences just the z-component of the noisy Overhauser field. Furthermore, the heavy-hole coupling coefficients are reduced with respect to the electron coupling coefficients: $A_{\mathrm{h},z}^{j}/A_{\mathrm{e}}^{j} \simeq -10\%$ (refs 8,10). The most important consequence of the Ising form is that application of a transverse magnetic field suppresses hole spin dephasing by the nuclear spins[8]. This is so effective that the hyperfine interaction is to all intents and purposes switched off for a pure heavy-hole spin[11].

A close-to-ideal heavy-hole state exists in unstrained, highly confined GaAs quantum wells[12,13]. Quantum dots however have mixed states. Even for an ideal quantum dot shape, symmetry does not prevent heavy-hole–light-hole coupling[14,15]. Heavy-hole–light-hole coupling is an experimental fact[16–19], revealed by deviations in the optical selection rules from the heavy-hole limit. For strained InGaAs quantum dots, the light hole accounts for 5–10% of the hole state[16,18,19].

The light-hole component in the quantum dot hole state has important consequences for the hole spin hyperfine coupling[10,11,20,21]. Additionally, admixture of the conduction *s* orbitals should be taken into account[11,20]: while *s* admixture is small on account of the fundamental energy gap of the semiconductor, it turns

[1]Department of Physics, University of Basel, Klingelbergstrasse 82, CH-4056 Basel, Switzerland. [2]Institut Lumière Matière (ILM), UMR5306 Université Lyon 1/CNRS, Université de Lyon, 69622 Villeurbanne Cedex, France. [3]Lehrstuhl für Angewandte Festkörperphysik, Ruhr-Universität Bochum, D-44780 Bochum, Germany. *e-mail: richard.warburton@unibas.ch

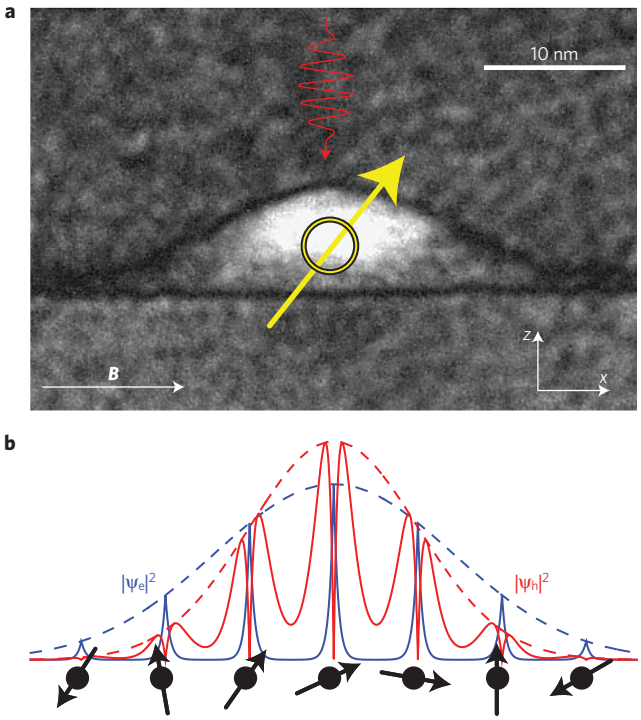

Figure 1 | Electron and hole wavefunctions. a, TEM image of a self-assembled quantum dot with a pictorial schematic of the experiment: a quantum dot loaded with a single hole is subject to an in-plane magnetic field (along the *x*-direction) and optical excitation (light propagating along the growth direction, *z*). **b**, Schematic of the electron and hole states. The electron state is constructed largely from atomic *s* orbitals, each localized to a unit cell (blue line) but shaped in amplitude by the envelope function that extends over the quantum dot (dashed line). In contrast, the hole state is constructed largely from atomic *p* orbitals (red line). The probability density for an electron to reside at the location of the nuclei (black circles) is therefore large for an electron, small for a hole. Ψ_e and Ψ_h denote the envelope functions for the electron and hole, respectively.

on the large Fermi contact part of the Hamiltonian. In a $\mathbf{k}\cdot\mathbf{p}$-description, the band admixtures are described by an 8×8 Hamiltonian (conduction, heavy-hole, light-hole and spin–orbit split-off states); the hyperfine interaction consists of a Fermi contact term and dipole–dipole-like interactions[8,10]. For the hole states, provided the admixtures of light-hole and conduction states are small, the hyperfine interaction can be folded down to an effective 2×2 Hamiltonian that operates on the mixed hole states (see Supplementary Information). The two mixed hole states are described as a spin-$\frac{1}{2}$ pseudospin, $\mathbf{S}$: $S_z=+1/2\equiv|\Uparrow\rangle$ represents one of the mixed states, $S_z=-1/2\equiv|\Downarrow\rangle$ represents the other. The final result (see Supplementary Information) is that the hole hyperfine interaction is no longer purely Ising-like:

$$H^h_{\rm hf}=\Omega\sum_{j=1}^{N}|\Psi_{\rm h}(\mathbf{R}_j)|^2(A^j_{{\rm h},z}I^j_zS_z+A^j_{{\rm h},x}I^j_xS_x+A^j_{{\rm h},y}I^j_yS_y) \qquad (3)$$

$A^j_{{\rm h},x}$ and $A^j_{{\rm h},y}$ are the transverse coupling coefficients and arise from the admixture of both conduction[11,20] and light-hole states[10,11,20,21], both couplings giving terms with the same functional form. In each case, $A^j_{{\rm h},x}$ and $A^j_{{\rm h},y}$ depend on $A^j_{{\rm h},z}$ multiplied by an admixture coefficient (see Supplementary Information). Any couplings to the $3d$ states also introduce a transverse hyperfine coupling[22,23]. The heavy-hole–light-hole coupling also introduces non-colinear terms[21] (see Supplementary Information). The transverse coupling makes the hole spin vulnerable to spin dephasing via the in-plane components of the nuclear spins, an interaction that cannot be suppressed in an in-plane magnetic field. In fact, the anisotropy (rather than the magnitude of $A^j_{{\rm h},z}$) represents a crucial issue in the development of a hole spin qubit.

Experiments have established long hole spin relaxation times[24–27], coherence times T_2 in the microsecond range[28,29], fast spin rotations[29–31] and control of two tunnel-coupled hole spin qubits[30]. The hole spin T_2 falls rapidly above 10 K, a consequence of a spin–orbit-mediated phonon interaction[32]. Conveniently, 4 K is cold enough to achieve a highly coherent hole spin. The existence of the longitudinal hole hyperfine interaction has been established[9]. Experimentally, $A^j_{{\rm h},z}$ averaged over the quantum dot, $\langle A_{{\rm h},z}\rangle$, has been measured to be -10% of the average value of A^e_i, $\langle A^e_i\rangle$, on self-assembled quantum dots by dynamically polarizing the nuclear spins along the z-direction and measuring the changes to the electron and hole Zeeman energies[33–35], confirming theoretical expectations[8,10] albeit with some interesting discussion on the sign[22,23]. However, the anisotropy of the hole hyperfine interaction has not yet been determined: it is at present unclear if the ideal heavy-hole limit can be reached with available quantum dots.

Two difficulties are encountered in probing the hole spin hyperfine interaction optically. First, optical excitation of a hole spin populates an exciton state consisting of two holes in a singlet state but an unpaired electron spin. In this situation it is not trivial to assign any nuclear spin effects unambiguously to the hole spin given the strong hyperfine interaction of the electron spin. Second, p-type devices tend to be considerably noisier than n-type devices yet the hole g-factor is very sensitive to an electric field[36–38] such that charge noise results in spin dephasing[29,37,38]: in noisy devices this effect completely obscures the hyperfine couplings.

Here we probe the hole hyperfine interaction in a self-assembled InGaAs quantum dot and uncover an extremely high anisotropy, that is, close-to-Ising-like, $\langle A_{{\rm h},x}\rangle \ll \langle A_{{\rm h},z}\rangle$. The first step is to reduce radically the charge noise in p-type devices. We achieve this by inverting the standard design, switching from a p–i–Schottky structure to an n–i–p device. The second step is to carry out an experiment that is sensitive to the transverse terms in the hole hyperfine interaction. We polarize the nuclear spins along a transverse direction, monitoring the polarization via the lone electron spin in the exciton, and measure the hole Zeeman splitting $Z_{\rm h}$ ultraprecisely by means of dark-state spectroscopy, that is, coherent population trapping (CPT)[28,37,39–41]. The combination of a coherent hole spin, resonance fluorescence detection[42] and low-noise samples enables us to achieve a spectral resolution in $Z_{\rm h}$ of just 10 neV (2.4 MHz). We demonstrate both a decoupling of the hole spin from the nuclei and a very small dephasing rate via charge noise leading to T_2^* times close to a microsecond. An InGaAs quantum dot therefore represents an attractive framework for a hole-based spin qubit.

Low-noise p-type device

Figure 2 shows the p–i–Schottky structure and the inverted structure, an n–i–p device (see also Supplementary Information). In each case the quantum dots are grown in the intrinsic region (see Methods). In the n–i–p structure, the p-doped layer acts as an 'epitaxial gate' and is grown last. This turns out to have a massive effect on the quality of the devices. The reason is threefold. First, growing a p^+-layer with C doping (C doping is vastly superior to Be doping as Be floats to the surface during growth resulting in optical broadenings and Fano effects[43]) involves heating the carbon cell to very large temperatures: this results in a degradation of the vacuum and a loss of quality of all material grown on top of the p^+-layer. Second, i-GaAs grown on top of p^+-GaAs has much poorer optical quality than i-GaAs grown on top of n^+-GaAs. This is probably related to the lattice defects in the p^+-layer leading to a broadband of states in the energy gap. Third, even weakly C-doped GaAs is problematic as the C atoms represent relatively deep trapping

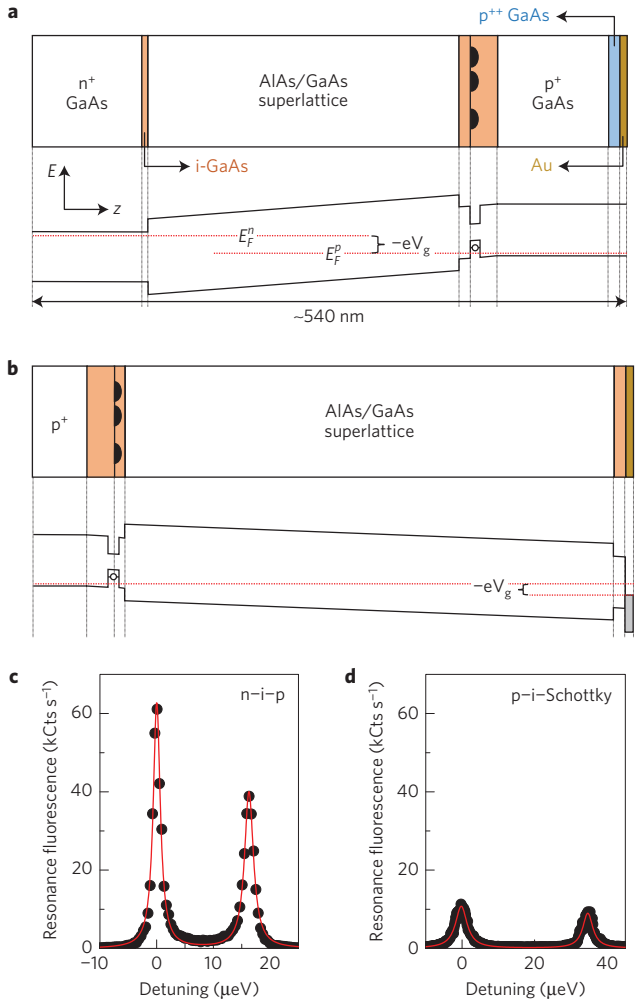

Figure 2 | Devices for loading a quantum dot with a single hole. a, n–i–p device. **b**, p–i–Schottky device: heterostructure design and schematic band diagram. **c**, Resonance fluorescence spectrum at 4.2 K on an empty quantum dot in the p–i–n device. The two lines (split by the exciton fine structure) have a linewidth of 1.5 μeV, equal to the linewidth in the very best n-type devices, demonstrating the extremely low level of charge noise. **d**, Resonance fluorescence spectrum at 4.2 K on an empty quantum dot in the p–i–Schottky device. The larger linewidths of 3.6 μeV and also the smaller signals signify problems related to the p-doping: increased charge noise and non-radiative decay.

centres[44]. By growing the p^+-layer last, these problems are avoided: high quality is locked into the i-GaAs. Additionally, an epitaxial gate is superior to a Schottky gate in other respects: it is lattice-matched and thus strain-free, monolithic, and highly transparent for optics; it has a well-defined potential step (in contrast to the Schottky barrier); it is grown *in situ* without prior exposure to air and moisture; it withstands higher reverse bias voltages; and it is thermally more stable than a Schottky gate. A point of detail concerns the capping layer, the i-GaAs grown between the quantum dot layer and the blocking barrier (an AlAs/GaAs superlattice). At intermediate thicknesses, fluctuating minority carriers at the GaAs/blocking barrier interface result in unwanted charge noise[45]. This noise can be suppressed by increasing the capping layer thickness, which increases the separation between quantum dots and the fluctuating charges[45,46]. An alternative is to make the capping layer thickness very small, pushing the minority charge states well above the quantum dot levels such that the states are unlikely to be occupied at low temperature. For the n–i–p structure, we choose a very small capping layer thickness, 10 nm, to suppress these space charge effects and also to prevent optically excited electrons from tunnelling out of the device.

To demonstrate the improvements on switching to the inverted structure, Fig. 2 shows low-temperature resonance fluorescence spectra of the neutral exciton on a quantum dot in a p–i–Schottky device and in an n–i–p device, both wafers consisting of extremely high-quality GaAs grown under the same conditions. Low-temperature resonance fluorescence (see Methods for experimental details) is an excellent probe of material quality: the linewidth is sensitive to charge noise via the large dc Stark shift; the relative intensity is sensitive to any non-radiative decay. The quantum dot in the p–i–Schottky device has an optical linewidth of 3.6 μeV (average in this wafer 4.1 ± 1.1 μeV), better than previous p–i–Schottky devices[25,28]. Significantly, the optical linewidth of the quantum dot in the n–i–p device reduces to just 1.5 μeV (average in this wafer 1.4 ± 0.3 μeV). The quantum dots in the n–i–p device work as well as our best n-type samples[46]. By determining quantitatively the contributions of charge noise and spin noise to the linewidth[46], we can conclude that the potential fluctuations at the location of the quantum dots amount to just $V_{\mathrm{r.m.s.}} = 1.2\,\mu\mathrm{V}$ (ref. 46).

Coherence population trapping on a single hole spin

CPT is our main spectroscopic tool to perform a high-resolution measurement of the hole Zeeman energy (see Methods). CPT is a quantum interference in a Λ-system where two ground states are coupled individually by 'pump' and 'probe' optical fields to a common upper level (Fig. 3a; see Supplementary Information). Here, the two ground states correspond to the Zeeman-split hole spin states, described as $|\Uparrow\rangle_x$ and $|\Downarrow\rangle_x$, and the upper level to an exciton, $|\Uparrow\downarrow,\downarrow\rangle_x$ or $|\Uparrow\downarrow,\uparrow\rangle_x$, where $|\Uparrow\rangle_x$ and $|\Downarrow\rangle_x$ are the eigenstates of the hole pseudospin in the x-basis (see Supplementary Information) and $|\uparrow\rangle_x, |\downarrow\rangle_x$ refer to the electron spin states, also in the x-basis (Fig. 3a). A transverse magnetic field (in the x-direction) establishes the quantization axis and the Λ-system (Fig. 3a). This applies to a hole spin provided the in-plane g-factor is non-zero: the interference occurs when the frequency difference of the lasers matches the hole Zeeman splitting, the two-photon resonance. A dark state results, revealed by a dip in the probe spectrum. The spectral position of the dip measures Z_h. Specifically, when $\hbar\Omega_1 \ll \hbar\Omega_2 \ll \hbar\Gamma_r$ ($\hbar\Omega_1, \hbar\Omega_2$ are the probe and pump couplings, Γ_r the spontaneous emission rate), the CPT dip has width $\hbar\Omega_2^2/\Gamma_r$. The depth of the dip is sensitive to the hole spin coherence: only for $1/T_2 \ll \Omega_2^2/\Gamma_r$ does the emission in the dip go to zero. Hence, provided the hole spin coherence is high enough, the width of the CPT dip can be much less than the optical linewidth, enabling a highly accurate measurement of Z_h. Furthermore, the location of the CPT dip is determined only by the two-photon resonance. CPT is therefore an ideal technique to extract Z_h. Fluctuations in exciton energy (via charge noise and the Overhauser field acting on the electron spin) modify the emission envelope[28,39] but not the location of the CPT dip.

CPT on a single quantum dot containing a single hole is shown in Fig. 3b. The new p-type devices are very important: they remove the charge-noise-induced fluctuations of the CPT dip position that plagued earlier experiments[37]. The occupation of the upper level is monitored with high signal/noise by detecting the resonance fluorescence[42,46] (Fig. 3b,c). The resonance fluorescence exhibits a Lorentzian envelope with full-width at half-maximum (FWHM) 2.5 μeV and a pronounced dip with FWHM 80 neV (19.3 MHz). A zoom-in of the CPT dip is shown in Fig. 3c along with CPT from a quantum dot in sample B with CPT dip width 33 neV (8.0 MHz). These spectra enable the determination of Z_h with a resolution of ~10 neV. We find that the hole g-factor (in-plane magnetic field) is $g_{h,x} = 0.063$ for quantum dot A, $g_{h,x} = 0.035$ for quantum dot B. Averaged over many quantum dots in these samples, $\langle g_{h,x}\rangle = 0.12 \pm 0.10$; in the vertical direction, the hole g-factor is much larger, $\langle g_{h,z}\rangle = 1.22 \pm 0.03$. This is reminiscent of the close-to-ideal heavy-hole state

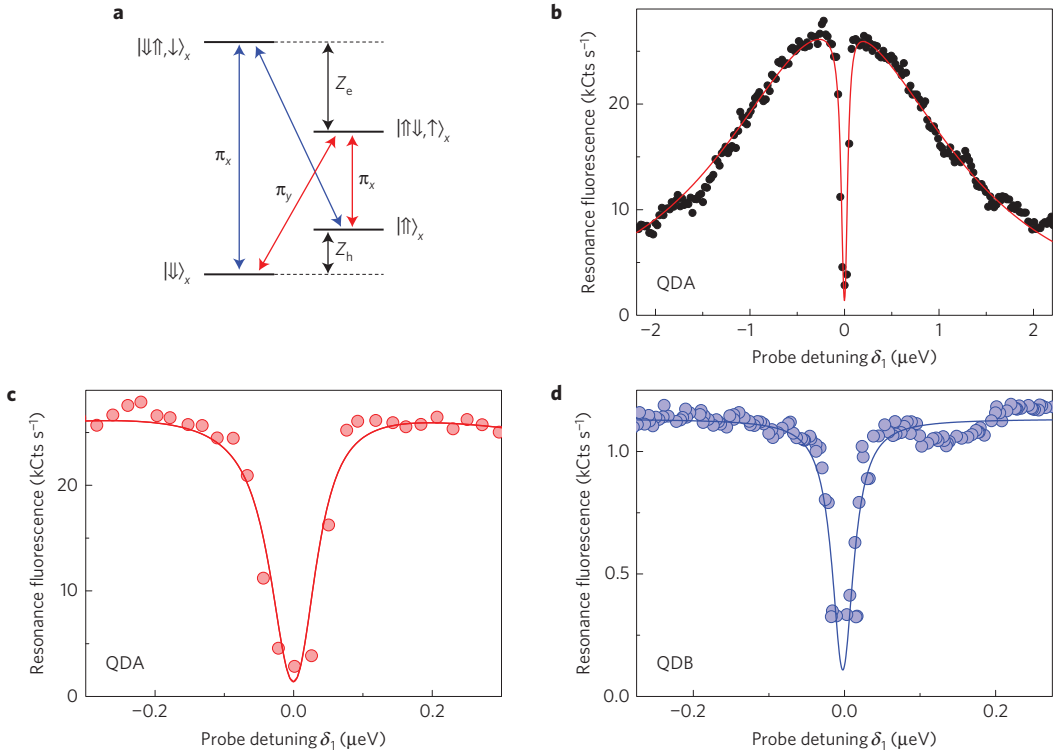

Figure 3 | Coherent population trapping on a single hole spin. a, The quantum states. Two optical Λ-systems (blue and red lines) are established in a magnetic field along the *x*-direction: $|\Uparrow\rangle_x$ and $|\Downarrow\rangle_x$ are the hole pseudospin eigenstates in the *x*-basis, split by the Zeeman energy Z_h; the upper levels are the X^{1+} excitons consisting of two holes in a singlet state and an unpaired electron with spin ±(1/2), again in the *x*-basis. The optical transitions are linearly polarized, either π_x or π_y, with equal optical dipoles, at wavelengths close to 950 nm. **b**, Resonance fluorescence spectrum on a single quantum dot QDA containing a single hole in sample A using the 'blue' Λ-system (pump on higher energy 'vertical' transition). The pronounced dip signifies CPT. The solid line shows the result of a three-level density matrix model (probe coupling $\hbar\Omega_1 = 0.06$ μeV, pump coupling $\hbar\Omega_2 = 0.40$ μeV, spontaneous emission rate $\Gamma_r = 0.68$ μeV, $T_2 > 1$ μs, $T_1 \gg T_2$) convoluted with a Lorentzian with FWHM $\Gamma = 2.5$ μeV to describe slow exciton dephasing, and then with a Lorentzian with FWHM 8.3 neV (2.0 MHz) to account for the mutual coherence of the lasers (see Supplementary Information). The data were recorded with 0.1 s integration time per point at a magnetic field $B_x = 3.00$ T and temperature $T = 4.2$ K. **c**,**d**, Two exemplary CPT dips of QDA and QDB, respectively. The dip from QDA has a FWHM of 80 neV (19.3 MHz) and is modelled with the parameters of **b**. The limited mutual coherence of the lasers is the main reason that the signal in the dip centre does not go down completely to zero. The dip from QDB has a FWHM of 33 neV (8.0 MHz), 5 s integration per point. The CPT simulation uses $\hbar\Omega_1 = 0.1$ μeV, $\hbar\Omega_2 = 0.49$ μeV and, as in **b**, $\Gamma_r = 0.68$ μeV, $T_2 > 1$ μs, $T_1 \gg T_2$. In this case, the remaining signal in the dip centre is likely to be a consequence of the small value of Z_h: the dark state can be destroyed by the weak coupling of the pump to the probe transition.

in an unstrained quantum well for which $g_{h,x} \ll g_{h,z}$. However, the magnitude of $g_{h,x}$ is an unreliable measure of the heavy-hole–light-hole admixture as $g_{h,x}$ is very sensitive to the indium concentration via the strong dependence of the band structure parameters on indium concentration[38]. A small $g_{h,x}$ is encouraging but in itself does not represent a suppressed hole spin hyperfine interaction.

The transverse hole hyperfine interaction

The transverse hole hyperfine interaction is measured by combining CPT and dynamic nuclear polarization (DNP). At zero magnetic field, the resonance fluorescence spectra have a straightforward Lorentzian lineshape. This can change in an applied magnetic field where the resonance has a 'top-hat' shape extending over tens of microelectronvolts and a strong hysteresis on reversing the scan direction[33,47,48]. The interpretation is that as the laser is tuned, the nuclei polarize in such a way that resonance with the laser is maintained. This effect, referred to as 'dragging', occurs also here and is used as a tool to create a large DNP. Dragging arises through the hyperfine interaction of the lone electron spin in the exciton. Furthermore, the exact change in electron Zeeman energy under DNP can be probed spectroscopically by measuring a change in transition energy of one of the exciton transitions.

In the experiment, the DNP is controlled via the detuning δ_2 of the pump laser with respect to the bare transition frequency. A strong constant frequency pump laser defines the nuclear spin state and a weak probe laser ($\Omega_1 \ll \Omega_2$) measures both Z_h and the electron Zeeman splitting Z_e. The probe laser is scanned across the vertical and diagonal transitions (Fig. 4a,b). A pronounced dip in the spectrum indicates CPT and measures Z_h with ultrahigh resolution. For zero pump detuning (zero DNP), the probe response at much lower frequencies determines Z_e: we observe an increase in resonance fluorescence when the probe comes into resonance with the lower energy 'vertical' exciton transition, $|\Uparrow\rangle_x \rightarrow |\Uparrow\Downarrow,\uparrow\rangle_x$ (Fig. 4a,b). As the pump is detuned, dragging causes Z_e to change and the change ΔZ_e can be simply monitored via a shift in the exciton transition (Fig. 4a,b). Importantly, the probe coupling is lowered in these experiments until the probe itself is too weak to induce DNP, that is, the frequency of the low-energy resonance does not depend on Ω_1. At each pump detuning, equivalently at each value of ΔZ_e, we determine the hole Zeeman energy Z_h with ultrahigh resolution by measuring the exact spectral location of the CPT dip (Fig. 4a; see Methods for fitting procedure). Figure 4c,d plots Z_h versus ΔZ_e. Although Z_e changes by almost 20 μeV, Z_h remains constant to within 20 neV for both quantum dots. This is the main result of the experiment: large values of $\langle I_x \rangle$ do not result in a measurable change in Z_h even when Z_h is measured with high resolution.

Quantitatively, our experiment shows that $|\Delta Z_h / \Delta Z_e| < 0.1\%$ in the presence of a transverse DNP. This result can be interpreted

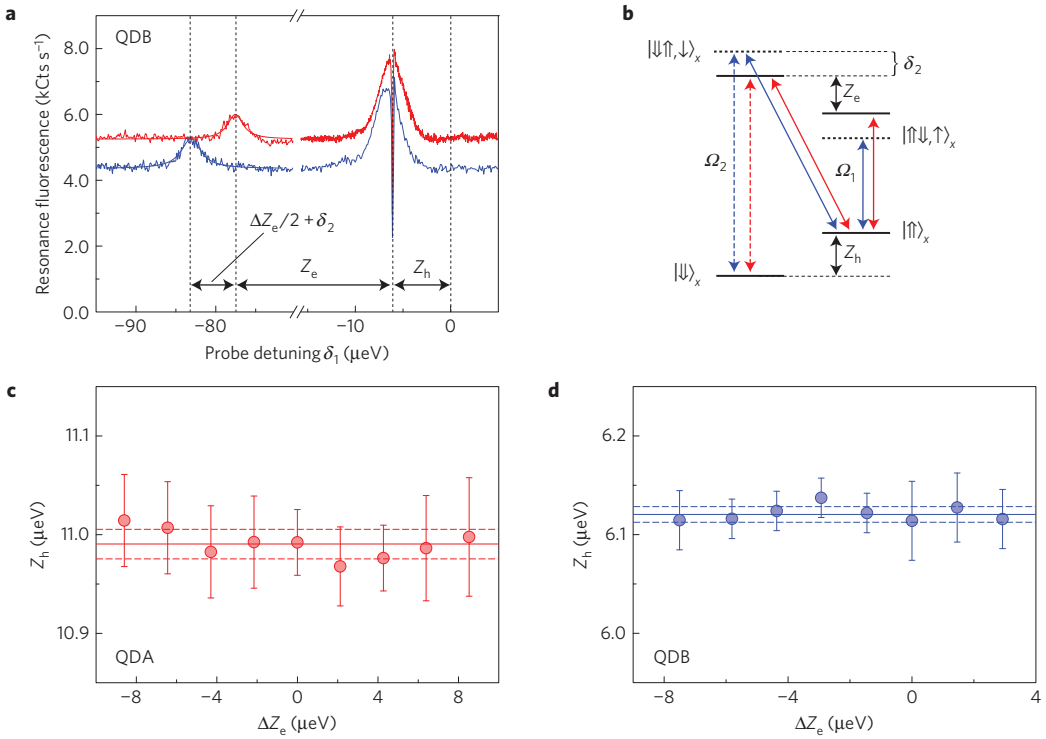

Figure 4 | The transverse hyperfine coupling of a single hole spin. a, Measured probe resonance fluorescence spectrum on QDB in the presence of a much stronger, constant frequency pump laser, red: $\delta_2 = 0$; blue: $\delta_2 = 3.4$ μeV. The frequency of the probe laser is scanned across the 'vertical' and 'diagonal' transitions and is plotted with respect to the pump frequency in both cases. The pronounced dip signifies CPT and occurs when $\delta_1 = Z_h$. The peak at large and negative δ_1 arises when the probe is in resonance with the lower energy 'vertical' transition. At $\delta_2 = 0$ the separation between this resonance and the CPT dip determines Z_e, the Zeeman energy of the exciton (determined by the lone electron spin). The shift in this resonance signifies a DNP: Z_e changes in response to the change in pump detuning. The measured Rabi energies are $\hbar\Omega_1 = 0.049$ μeV and $\hbar\Omega_2 = 0.49$ μeV; magnetic field 3.00 T; integration time per point 5 s; temperature 4.2 K. **b**, The quantum states of the system. The red arrows indicate the optical transitions addressed by scanning the probe laser for $\delta_2 = 0$, blue for $\delta_2 > 0$. **c**,**d**, Z_h versus the change of the electron Zeeman energy ΔZ_e for samples A (*g*-factor 0.063) and B (*g*-factor 0.035), respectively. The solid line represents the average value; the dashed lines represent $\pm\sigma$ where σ is the standard deviation. At the one-σ level, $dZ_h/d\Delta Z_e = 0.1\%$.

in terms of averaged hyperfine couplings, $\Delta Z_h/\Delta Z_e \simeq \langle A_{h,x}\rangle/\langle A_e\rangle$ (see Supplementary Information). Hence, $|\langle A_{h,x}\rangle/\langle A_e\rangle| < 0.1\%$. Furthermore, with $|\langle A_{h,z}\rangle/\langle A_e\rangle| = 10\%$ (refs 33–35; a ratio we have confirmed on quantum dots in these samples), we can quantify the anisotropy of the hole spin hyperfine interaction $|\langle A_{h,x}\rangle/\langle A_{h,z}\rangle| < 1\%$. This is consistent both with our estimates of the heavy-hole–light-hole mixing in these quantum dots (see Supplementary Information) and with generic theoretical estimates[11,21]; a full calculation specific to an InGaAs quantum dot including all admixtures is at present lacking. In terms of energies, $|\langle A_{h,x}\rangle| < 0.1$ μeV. This implies a very small energy broadening δZ_h in the presence of unpolarized but noisy nuclei ($\delta Z_e = 600$ neV): $\delta Z_h^{spin} < 0.6$ neV. The energy broadening arising from the longitudinal coupling, that is, from $\langle A_{h,z}\rangle$, is subnanoelectronvolt for all transverse fields above about 500 mT.

Hole spin dephasing

We determine T_2^* in these experiments. In a CPT experiment, ensemble broadening (described with a T_2^* time, $T_2^* = \hbar/\delta Z_h$) reveals itself by a lifting of the signal in the dip away from zero and an increase in the dip width. An analysis of the CPT spectra of Fig. 3, taking into account the mutual coherence of the lasers, results in an energy broadening $\delta Z_h = 3.3 \pm 2.2$ neV. T_2^* is so large that it is very challenging to measure it with small error. To reduce the error, we complement the CPT result with all of the other spectroscopic results. First, we evaluate the contribution to δZ_h from charge noise. We determine *in situ* the r.m.s. voltage fluctuations from the X^0 linewidth; we measure *in situ* the sensitivity of the hole spin to a voltage fluctuation by recording the voltage dependence of the hole Zeeman energy. Charge noise is particularly small on sample A contributing 0.10 ± 0.05 μeV to the optical linewidth[49]. We find that charge noise results in a Z_h fluctuation of $\delta Z_h^{charge} = 0.3$ neV at $B_x = 3.00$ T. Second, we evaluate the contribution to δZ_h from spin noise in the actual experiment. In this case, the X^{1+} linewidth measures the r.m.s. fluctuations in electron Zeeman energy, $\delta Z_e = 1.43 \pm 0.07$ μeV at $B_x = 3.00$ T. This noise arises from a fluctuation in the nuclear spin polarization projected along x, the magnetic field direction, and it corresponds to an Overhauser field of ~ 40 mT. This value demonstrates that we do not 'narrow' the nuclear spin distribution in this experiment. From our upper limit on the coupling coefficient, the corresponding fluctuations in Z_h amount to $< 1.43 \pm 0.25$ neV. These results from the linewidths are completely consistent with the CPT result. The final result is that $T_2^* > (460 \pm 80)$ ns.

The long value of hole spin T_2^* arises from the application of an in-plane magnetic field to suppress the longitudinal hyperfine interaction; a very small transverse hyperfine interaction; and low levels of charge noise to reduce charge-noise-induced dephasing. We note that our value for T_2^* is considerably larger than reported in other experiments[29–31]: we propose that this is entirely related to the different levels of charge noise. T_2^* is limited by charge and spin noise. In both cases, most of the noise lies at frequencies below 100 kHz (ref. 46) such that dynamical decoupling schemes are likely to be highly effective at prolonging the usable coherence beyond T_2^*. Additionally, the nuclear spin coupling can be reduced even further by fabricating flatter quantum dots with circular cross-section to reduce the heavy-hole–light-hole admixture. A realistic prospect is to push T_2^* into the microsecond regime. As for a quantum dot

electron spin[50], a quantum dot hole spin can be rotated in ∼10 ps (refs 29–31). This combination makes the hole spin in an InGaAs quantum dot an attractive platform.

Methods

Methods and any associated references are available in the online version of the paper.

Received 28 April 2015; accepted 21 June 2016; published online 25 July 2016

References

1. Loss, D. & DiVincenzo, D. P. Quantum computation with quantum dots. *Phys. Rev. A* **57,** 120–126 (1998).
2. Merkulov, I. A., Efros, A. L. & Rosen, M. Electron spin relaxation by nuclei in semiconductor quantum dots. *Phys. Rev. B* **65,** 205309 (2002).
3. Khaetskii, A. V., Loss, D. & Glazman, L. Electron spin decoherence in quantum dots due to interaction with nuclei. *Phys. Rev. Lett.* **88,** 186802 (2002).
4. Warburton, R. J. Single spins in self-assembled quantum dots. *Nature Mater.* **12,** 483–493 (2013).
5. Saeedi, K. *et al*. Room-temperature quantum bit storage exceeding 39 minutes using ionized donors in silicon 28. *Science* **342,** 830–833 (2013).
6. Kawakami, E. *et al*. Electrical control of a long-lived spin qubit in a Si/SiGe quantum dot. *Nature Nanotech.* **9,** 666–670 (2014).
7. Grncharova, E. & Perel, V. Relaxation of nuclear spins in interacting with holes in semiconductors. *Sov. Phys. Semicond.* **11,** 977–1000 (1977).
8. Fischer, J., Coish, W. A., Bulaev, D. V. & Loss, D. Spin decoherence of a heavy hole coupled to nuclear spins in a quantum dot. *Phys. Rev. B* **78,** 155329 (2008).
9. Eble, B. *et al*. Hole-nuclear spin interaction in quantum dots. *Phys. Rev. Lett.* **102,** 146601 (2009).
10. Testelin, C., Bernardot, F., Eble, B. & Chamarro, M. Hole-spin dephasing time associated with hyperfine interaction in quantum dots. *Phys. Rev. B* **79,** 195440 (2009).
11. Fischer, J. & Loss, D. Hybridization and spin decoherence in heavy-hole quantum dots. *Phys. Rev. Lett.* **105,** 266603 (2010).
12. van Kesteren, H. W., Cosman, E. C., van der Poel, W. A. J. A. & Foxon, C. T. Fine structure of excitons in type-II GaAs/AlAs quantum wells. *Phys. Rev. B* **41,** 5283–5292 (1990).
13. Martin, R. W. *et al*. Two-dimensional spin confinement in strained-layer quantum wells. *Phys. Rev. B* **42,** 9237–9240 (1990).
14. Bester, G. & Zunger, A. Cylindrically shaped zinc-blende semiconductor quantum dots do not have cylindrical symmetry: atomistic symmetry, atomic relaxation, and piezoelectric effects. *Phys. Rev. B* **71,** 045318 (2005).
15. Luo, J.-W., Bester, G. & Zunger, A. Supercoupling between heavy-hole and light-hole states in nanostructures. *Phys. Rev. B* **92,** 165301 (2015).
16. Krizhanovskii, D. N. *et al*. Individual neutral and charged $In_xGa_{1-x}As$-GaAs quantum dots with strong in-plane optical anisotropy. *Phys. Rev. B* **72,** 161312 (2005).
17. Belhadj, T. *et al*. Impact of heavy hole-light hole coupling on optical selection rules in GaAs quantum dots. *Appl. Phys. Lett.* **97,** 051111 (2010).
18. Dreiser, J. *et al*. Optical investigations of quantum dot spin dynamics as a function of external electric and magnetic fields. *Phys. Rev. B* **77,** 075317 (2008).
19. Lu, C.-Y. *et al*. Direct measurement of spin dynamics in InAs/GaAs quantum dots using time-resolved resonance fluorescence. *Phys. Rev. B* **81,** 035332 (2010).
20. Maier, F. & Loss, D. Effect of strain on hyperfine-induced hole-spin decoherence in quantum dots. *Phys. Rev. B* **85,** 195323 (2012).
21. Ribeiro, H., Maier, F. & Loss, D. Inhibition of dynamic nuclear polarization by heavy-hole noncollinear hyperfine interactions. *Phys. Rev. B* **92,** 075421 (2015).
22. Chekhovich, E. A. *et al*. Nuclear spin effects in semiconductor quantum dots. *Nature Mater.* **12,** 494–504 (2013).
23. Chekhovich, E. A. *et al*. Element-sensitive measurement of the hole-nuclear spin interaction in quantum dots. *Nature Phys.* **9,** 74–78 (2013).
24. Heiss, D. *et al*. Observation of extremely slow hole spin relaxation in self-assembled quantum dots. *Phys. Rev. B* **76,** 241306 (2007).
25. Gerardot, B. D. *et al*. Optical pumping of a single hole spin in a quantum dot. *Nature* **451,** 441–444 (2008).
26. Li, Y. *et al*. Intrinsic spin fluctuations reveal the dynamical response function of holes coupled to nuclear spin baths in (In,Ga)As quantum dots. *Phys. Rev. Lett.* **108,** 186603 (2012).
27. Dahbashi, R., Hübner, J., Berski, F., Pierz, K. & Oestreich, M. Optical spin noise of a single hole spin localized in an (InGa)As quantum dot. *Phys. Rev. Lett.* **112,** 156601 (2014).
28. Brunner, D. *et al*. A coherent single-hole spin in a semiconductor. *Science* **325,** 70–72 (2009).
29. De Greve, K. *et al*. Ultrafast coherent control and suppressed nuclear feedback of a single quantum dot hole qubit. *Nature Phys.* **7,** 872–878 (2011).
30. Greilich, A., Carter, S. G., Kim, D., Bracker, A. S. & Gammon, D. Optical control of one and two hole spins in interacting quantum dots. *Nature Photon.* **5,** 702–708 (2011).
31. Godden, T. M. *et al*. Coherent optical control of the spin of a single hole in an InAs/GaAs quantum dot. *Phys. Rev. Lett.* **108,** 017402 (2012).
32. Varwig, S. *et al*. Temperature dependence of hole spin coherence in (In,Ga)As quantum dots measured by mode-locking and echo techniques. *Phys. Rev. B* **87,** 115307 (2013).
33. Fallahi, P., Yilmaz, S. T. & Imamŏglu, A. Measurement of a heavy-hole hyperfine interaction in InGaAs quantum dots using resonance fluorescence. *Phys. Rev. Lett.* **105,** 257402 (2010).
34. Chekhovich, E. A., Krysa, A. B., Skolnick, M. S. & Tartakovskii, A. I. Direct measurement of the hole-nuclear spin interaction in single InP/GaInP quantum dots using photoluminescence spectroscopy. *Phys. Rev. Lett.* **106,** 027402 (2011).
35. Kurtze, H., Yakovlev, D. R., Reuter, D., Wieck, A. D. & Bayer, M. Hyperfine interaction mediated exciton spin relaxation in (In,Ga)As quantum dots. *Phys. Rev. B* **85,** 195303 (2012).
36. Bennett, A. J. *et al*. Voltage tunability of single-spin states in a quantum dot. *Nature Commun.* **4,** 1522 (2013).
37. Houel, J. *et al*. High resolution coherent population trapping on a single hole spin in a semiconductor quantum dot. *Phys. Rev. Lett.* **112,** 107401 (2014).
38. Prechtel, J. H. *et al*. Electrically tunable hole *g* factor of an optically active quantum dot for fast spin rotations. *Phys. Rev. B* **91,** 165304 (2015).
39. Fleischhauer, M., Imamoglu, A. & Marangos, J. P. Electromagnetically induced transparency: optics in coherent media. *Rev. Mod. Phys.* **77,** 633–673 (2005).
40. Xu, X. *et al*. Coherent population trapping of an electron spin in a single negatively charged quantum dot. *Nature Phys.* **4,** 692–695 (2008).
41. Hansom, J. *et al*. Environment-assisted quantum control of a solid-state spin via coherent dark states. *Nature Phys.* **10,** 725–730 (2014).
42. Kuhlmann, A. V. *et al*. A dark-field microscope for background-free detection of resonance fluorescence from single semiconductor quantum dots operating in a set-and-forget mode. *Rev. Sci. Instrum.* **84,** 073905 (2013).
43. Gerardot, B. D. *et al*. Laser spectroscopy of individual quantum dots charged with a single hole. *Appl. Phys. Lett.* **99,** 243112 (2011).
44. Hauck, M. *et al*. Locating environmental charge impurities with confluent laser spectroscopy of multiple quantum dots. *Phys. Rev. B* **90,** 235306 (2014).
45. Houel, J. *et al*. Probing single-charge fluctuations at a GaAs/AlAs interface using laser spectroscopy on a nearby InGaAs quantum dot. *Phys. Rev. Lett.* **108,** 107401 (2012).
46. Kuhlmann, A. V. *et al*. Charge noise and spin noise in a semiconductor quantum device. *Nature Phys.* **9,** 570–575 (2013).
47. Latta, C. *et al*. Confluence of resonant laser excitation and bidirectional quantum-dot nuclear-spin polarization. *Nature Phys.* **5,** 758–763 (2009).
48. Högele, A. *et al*. Dynamic nuclear spin polarization in the resonant laser excitation of an InGaAs quantum dot. *Phys. Rev. Lett.* **108,** 197403 (2012).
49. Kuhlmann, A. V. *et al*. Transform-limited single photons from a single quantum dot. *Nature Commun.* **6,** 8204 (2015).
50. Press, D., Ladd, T. D., Zhang, B. & Yamamoto, Y. Complete quantum control of a single quantum dot spin using ultrafast optical pulses. *Nature* **456,** 218–221 (2008).

Acknowledgements

We acknowledge financial support from NCCR QSIT, SNF project 200020_156637 and EU FP7 ITN S^3NANO. We thank F. Maier, H. Ribeiro, P. Szumniak, V. Kornich and D. Loss for fruitful discussions; J.-M. Chauveau for helping to perform the TEM shown in Fig. 1a; and S. Martin and M. Steinacher for technical support. A.L. and A.D.W. acknowledge gratefully support from DFH/UFA CDFA05-06, DFG TRR160 and BMBF Q.com-H 16KIS0109.

Author contributions

J.H.P., A.V.K. and J.H. performed the experiments and data analysis. A.L. and A.D.W. carried out the molecular beam epitaxy and sample fabrication. A.L. performed the TEM shown in Fig. 1a. J.H.P., A.V.K. and R.J.W. took the lead in writing the paper. R.J.W. conceived and managed the project.

Additional information

Supplementary information is available in the online version of the paper. Reprints and permissions information is available online at www.nature.com/reprints. Correspondence and requests for materials should be addressed to R.J.W.

Competing financial interests

The authors declare no competing financial interests.

Methods

The InGaAs quantum dots are grown by a Stranski–Krastanov self-assembly process. They emit around 950 nm wavelength. The hole is strongly confined: the hole–hole on-site Coulomb interaction is ∼25 meV. The quantum dots are embedded in vertical tunnelling structures to control the charge via Coulomb blockade. Sample A is an n–i–p device, and sample B is a p–i–Schottky device, both with 25 nm tunnel barriers (see Supplementary Information). The CPT experiment involves driving the optical resonances of a single quantum dot resonantly with two continuous wave lasers, 'pump' and 'probe', with a mutual coherence of 2.2 MHz. Both pump and probe lasers are stabilized in intensity; the pump laser is stabilized in frequency. Both pump and probe are linearly polarized at an angle of 45° to the direction of the magnetic field (applied along one of the crystal directions); resonance fluorescence is detected as the probe frequency is scanned, detecting with the orthogonal polarization to reject scattered laser light (a dark-field technique[42,46]). The optical couplings Ω are determined from the laser power once the link between laser power and Ω has been established by measuring power broadening at large Ω (see Supplementary Information).

The hole Zeeman energy Z_h is determined by fitting the data in the CPT dip to a Lorentzian function; the electron Zeeman energy Z_e is determined by fitting the data at the $|\Uparrow\rangle_x \rightarrow |\Uparrow\Downarrow,\uparrow\rangle_x$ transition, again to a Lorentzian function. CPT is simulated with the density matrix formalism applied to a three-level system including the pump and probe couplings and decay processes with the Lindblad approach (see Supplementary Information). The fluctuations in the CPT dip position and also the mutual coherence of the lasers are included by convoluting the result with a Lorentzian probability distribution.